Submitted, accepted and published by
J.HAZARDOUS MATERIALS 260:247– 254, 2013

Influence of temperature and regeneration cycles on Hg capture and efficiency by structured Au/C regenerable sorbents.

D. Ballestero[1], C. Gómez-Giménez[2], E. García-Díez[2], R. Juan[2], B. Rubio[2], M.T. Izquierdo[2*]

[1] Universidad San Jorge. Autovía A23 Zaragoza-Huesca km 510. 50830 Villanueva de Gállego, Zaragoza. Spain.

[2] Instituto de Carboquímica, ICB-CSIC. c/Miguel Luesma Castán, 4. 50018 Zaragoza. Spain.

* Corresponding author e-mail: mizq@icb.csic.es

ABSTRACT

The objective of this work is to evaluate a novel regenerable sorbent for mercury capture based on gold nanoparticles supported on a honeycomb structured carbon monolith. A new methodology for gold nanoparticles deposition onto carbon monolith support has been developed to obtain an Au sorbent based on the direct reduction of a gold salt onto the carbon material. For comparison purposes, colloidal gold method was also used to obtain Au/C sorbents. Both types of sorbents were characterized by different techniques in order to obtain the bulk gold content, the particle size distribution and the chemical states of gold after deposition. The mercury capture capacity and mercury capture efficiency of sorbents were tested in a bench scale facility at different experimental conditions. The regenerability of the sorbents was tested along several cycles of mercury capture regeneration. High retention efficiencies are found for both types of sorbents comparing their gold content. Moreover, the high retention efficiency is maintained along several cycles of Hg capture-regeneration. The study of the fresh sorbent, the sorbent after Hg exposition and after regeneration by XPS and XRD gives insight to explain those results.

Keywords: mercury capture, regenerable sorbent, Au nanoparticles, carbon monolith

INTRODUCTION

Mercury is a leading concern among the air toxic metals because of its volatility, persistence, bioaccumulation in the environment and its neurological health impacts [1].

By far, the largest anthropogenic source of mercury is the burning of fossil fuels, primarily coal. Electrical power plants are estimated to account for about 25% of the global anthropogenic mercury emissions to the atmosphere and industrial and residential heating for another 20% [1].

Mercury present in coals varies widely based on its origin (where it was excavated) and any processes it undergoes prior to sale on the market. A literature review provides data of the mercury content of different coals [2]. Recent data reported in this review ranges mercury content between 0.05-0.35 mg/kg, with most values below 0.2 mg/kg.

During the combustion processes, these forms evaporate, giving rise to Hg^0, HgO and $HgCl_2$, which proportions in gas phase depend on the concentration and mode of occurrence in the coal and on the compounds present in the gaseous stream, especially particulates and HCl [3]. In pulverized-coal power plants more than 90% of the Hg in coal can be emitted in gas phase through the stack, in some cases. If the power plant has a wet flue gas desulphurization unit implemented (WFGD) [4], part of the oxidized mercury is removed in it, resulting in an average mercury emission to stack 25% Hg^{2+}:75% Hg^0.

The environmental implications of mercury do not correspond only to the emissions to the atmosphere; the quality of CO_2 to be transported and sequestered has been subject of research, concerning trace quantities of heavy metals participating in

mineralization and precipitation reactions in sequestration conditions. Moreover, mercury could accumulate within the CO_2 processing unit (CO_2 clean up and compression). The removal of Hg is necessary to protect key components in the CO_2 processing unit in order to prevent Hg attack on the aluminum heat exchangers. Mercury control post-combustion technologies can be associated with abatement measures for other pollutants (principally particulate and sulphur dioxide) [2, 5]. Mercury is adsorbed on fly ash, which is captured in the particulate matter control devices. Oxidized mercury can be absorbed in the scrubbing solution meanwhile elemental mercury is insoluble and cannot be captured. Average total mercury capture by existing ESP+WFGD varies depending on coal range, being for subbituminous coal about 30% [5]. These procedures generate residues that can be toxic, or of limited reutilization due to the presence of Hg (fly ashes in the PM control systems or gypsum retained in the scrubbers).

Specific technologies for mercury capture are mainly based on the use of sorbents injected in the gaseous stream for Hg capture, and subsequently retained in the particulate matter control systems, rendering new toxic residues to be controlled [6]. Activated carbon injection (ACI) technologies require a high C:Hg ratio to achieve the desired mercury removal level (> 90%), which results in a high portion cost for sorbent material. A major problem associated with ACI technology is that the commercial value of fly ash is sacrificed due to its mixing with contaminated activated carbon powder and the generation of high amount of toxic residue.

Regenerable sorbents can accomplish high mercury retention that can be recovered as well as balance cost because of its regenerability. Recognizing reversible characteristics of mercury amalgamate with gold and silver, gold- or silver-coated silica beads have been widely used to pre-concentrate low concentration of

elemental mercury for its detection [7, 8]. The gold- or silver-mercury amalgam is extremely stable at room temperature. However, the amalgam decomposes to release mercury to a gas phase at higher temperatures, leaving clean gold or silver surfaces ready for further mercury capture [8]. To effectively collect trace amounts of mercury, it is necessary to have the gold and/or silver in a form of large surface areas. However, metal monolayer tends to aggregate into larger islands in micrometer sizes after repetitive Hg exposure and heating, which could lead to inefficient mercury capture [8-10]. The efficiency of the Au for the retention of mercury would be enhanced if nanometric particulate sizes of the metal could be achieved.

Present work focuses on a structured Au/C regenerable sorbent, based on two different procedures for gold deposition on a carbon monolith: (i) colloidal gold method and (ii) gold salt method.

The first procedure use the traditional method based on citrate to produce gold nanoparticles [11]. This well-known method to get colloidal Au is fully in force for the preparation of catalysts with highly dispersed Au supported nanoparticles supported [12].

The second procedure to deposite nanometric gold, the salt method, is a novel concept for Au deposition. The reduction potential of the own carbon material is used to reduce Au^{3+} to Au^{0}. This hypothesis has been tested previously by the authors [13]. This method does not use other chemicals than the gold salt, and the gold nanoparticles are formed in-situ over the carbon support.

In this work, Au/C sorbents prepared following both methodologies for gold deposition were tested for mercury capture at different temperatures of operation in order to have a first approach to test different position in a coal power plant (ESP

cold-side, after WFGD or before the stack). Moreover, the regenerability of the novel sorbent (prepared with the gold salt method) was tested along several cycles of capture-regeneration.

EXPERIMENTAL

Preparation of sorbents

A commercial carbon monolith with honeycomb structure and square channel with a density 69 cell/cm^2 was used as support for gold deposition. Block of carbon material was cut and smoothed to obtain rectangular prisms with 36 channels, 15 mm length and 7x7 mm section. This support was used without treatment for direct gold deposition or treated with HNO_3 (acid concentration 65%, 80ºC, 4h) for colloidal gold deposition.

Two different methods for gold deposition onto the supports have been used. The first method for gold deposition consists of the direct reduction of the gold salt by the own carbon material of the support. The salt used for gold deposition was $HAuCl_4 \cdot 3H_2O$. A solution of 40 mg/l of salt in ethanol/water (1:1 v/v) was forced to pass through the channels of the carbon monolith to try to achieve a homogeneous deposition of gold along the channels of the monolithic supports. The contact time of the dissolution passing through the channels of the monolith was 30 min. The second method is based on the formation of colloidal gold [11] with the modification of reference [14]. During the formation of colloidal gold, citrate anion acts as reducing agent of the gold salt and as protector of the gold sol formed preventing its aggregation. The colloidal solution of gold is forced to pass through the channels,

with a total contact time between channels of the monoliths and the colloidal solution of 40 min.

After gold deposition distillated water was pumped through the channels of the sorbents to remove the spare gold dissolution. Sorbents were vacuum dried at 30ºC for 30 min. Sorbents were finally undergone to a reducing thermal treatment (TTR) at 300ºC in a flow containing 4%H_2 in N_2 during 1 h. Sorbents obtained by direct reduction of gold or by deposition of colloidal gold were labeled as MC-Au-red and MC-Au-col, respectively.

Characterization of sorbents

Sorbents were characterized by different techniques. A detailed description is given in reference [15]. The bulk Au content of the sorbents was obtained by Inductively Coupled Plasma Optical Emission Spectroscopy (ICP-OES). The surface Au content was determined by Scanning Electron Microscopy with Energy Dispersive X-ray Spectroscopy (SEM-EDX). The gold nanoparticle size distribution was obtained by image analysis (free software “Image J”) of electron micrographs taken by Scanning Electron Microscopy with Field-Emission (FE-SEM) technique. The oxidation states of gold were analyzed by X-ray Photoelectron Spectroscopy (XPS).

After mercury retention, some sorbents were characterized by XPS, in order to detect possible changes in Au oxidation state and X-ray Diffraction (XRD) in order to test crystal modification of Au by Au-Hg alloy formation.

Mercury capture and regeneration tests

A bench scale installation was used to determine the efficiency of the sorbents for the capture of mercury as well as the maximum retention capacity. A permeation tube for mercury gives the desired Hg concentration. The reactor is a quartz tube of 300 mm length with an internal diameter of 16 mm. The monolith is fitted inside using ceramic pieces. The mercury is analyzed on-line with an elemental mercury analyzer (VM3000). Moreover, the installation is provided with a tail-end train of flasks to allow the capture the mercury as well as its speciation (in the case of evidences of oxidation under the experimental conditions). The installation is built up with Teflon pipes and pieces (in the part of the installation where Hg is present) to prevent possible mercury attack to steel. More details of the experimental installation are given elsewhere [15].

The Hg breakthrough curves were obtained at a ratio W_{Au}/Q of $2.9x10^{-5}$ g h l^{-1} (where W_{Au} is the weight of Au used in each experiment and Q is the total gas flow), temperatures from 50ºC to 150ºC and Hg inlet concentration of 200 $\mu g/m^3$ in N_2. It was considered that saturation is reached at 95% breakthrough. Moreover, the amount of Hg retained at 20% and 80% of breakthrough was calculated from the integration of the breakthrough curve. The efficiency of Hg retention was calculated as the ratio between the amount of Hg retained by the sorbents at either 20% or 80% of breakthrough and the total amount of Hg fed into the reaction during this time. Some experiments were repeated to test reproducibility. Some of the exhausted sorbents after Hg capture were analyzed for Hg content in an automated mercury analyzer (AMA) from Leco, and the results were compared with those obtained by breakthrough curve integration.

Regeneration of exhausted sorbents was carried out at 220ºC during 1h. Details of the regeneration process are given in reference [15]. After this period of time, the

sorbent is cooled down to the desired temperature to be used in a new Hg capture test. Several cycles capture-regeneration were performed in order to test the efficiency for Hg retention along cycles.

RESULTS AND DISCUSSION

Honeycomb structured carbon monoliths have square channels with a density 69 cell/cm^2. This structure shows a very low pressure drop, high surface area to volume ratio and avoids particle entrainment. However, gold deposition on this structure has some difficulties regarding gold particles distribution homogeneity. So, definitive deposition procedure for both gold deposition methodologies considers homogeneity as well as reproducibility.

The gold content in the bulk sorbent was determined by ICP-OES and it was 0.110% for sorbent MC-Au-red and 0.035% for sorbent MC-Au-col.

The study of the distribution of gold along the monolith channels was carried out by SEM-EDX. Monoliths were longitudinal sectioned in order to determine the Au distribution along the channels. Seven measurement of gold content along each channel was carried out and an appropriate homogeneity of Au content was found. Moreover, different channels of a monolith and different monoliths were tested to obtain a representative value for Au surface content. The surface gold content from SEM-EDX for sorbent MC-Au-red was 3.96% and for MC-Au-col was 1.92%.

The study of the oxidation states of deposited gold before and after of TTR was carried out by XPS. The CASA data processing software allowed smoothing, Shirley type background subtraction, peak fitting and quantification. Binding energy regimes containing the Au $4f_{5/2}$ y Au $4f_{7/2}$ emission lines are presented in Figure 1. The fitting

of the Au 4f peaks was performed according contributions of different gold species [16-18]. The fitting shows the presence of various contributions with BEs that are given in Table 1. The doublet with peaks around 84.0 and 87.7 eV is characteristic of metallic gold. Peaks around 85.0 and 88.7 eV can be assigned to ionic species $Au^{\delta+}$. Before the TTR of the sorbents remaining oxidized Au can be found: 20.8% and 14.6% of the deposited gold for MC-Au-red and MC-Au-col, respectively. After reduction, the amount of oxidized gold decreases, and it is 12.2% and 11.3% of the deposited gold for MC-Au-red and MC-Au-col, respectively. Some studies reports that complete reduction is achieved as temperatures as high as 500ºC [19].

As the active specie for Hg amalgamation is Au^0, it means that this portion of oxidized Au will not participate on the Hg retention. However, for calculations bulk Au content was considered because the percentage of oxidized Au is similar for both sorbents. On the other hand, the gold content by XPS is referred to a spot of about 2 mm whereas bulk Au content is obtained by the analysis of a whole Au/C monolith and the value is an average of the Au analysis of three Au/C monoliths. The Au content before TTR is lower than after TTR, by XPS. This fact can be explained as after TTR the surface of Au particles are clean and “visible” for the analysis.

The importance of TTR is not only because the reduction of gold, but also because of temperature. As can be seen in Figure 2, the morphology of Au particles changes after TTR. The use of these sorbents along several cycles is based on the regeneration step in which mercury is released from the sorbent and the sorbent is ready for a new capture cycle. The temperature for Hg evolution from these sorbents is around 220ºC [15], so sorbents should be treated at least this temperature before using them for Hg capture-regeneration.

In order to obtain the gold particle size distribution on the sorbents, several micrographs were taken by FE-SEM in backscattering mode. Micrographs for MC-Au-red and MC-Au-col sorbents (after TTR) are shown in Figure 3. These micrographs were analyzed by image analysis using Image J free software.

The images show that the particles are well separated and dispersed, but the particle size distribution is quite different. With the colloidal gold method, the negatively-charged citrate ions are adsorbed onto the gold nanoparticles, introducing the surface charge that repels the particles and prevent them from aggregation. However, with the direct reduction method there is a spontaneous gold particle formation onto the carbon material due to the reduction potential of the own carbon material to reduce Au^{3+}. However, particle nucleation on carbon material is fast and ceases in a very short time, after which particle growth, rather than further nucleation, dominates. Therefore, the process needs a fine control to prevent the formation of high particle size or particle aggregation. These two mechanisms could explain the differences in Au particle size distribution, as can be seen in Figure 3. Average particle size (Feret's diameter) was 23 nm for sorbent MC-Au-red and 30 nm for sorbent MC-Au-col. These values were obtained by average of 286 and 1964 particles for MC-Au-red and MC-Au-col, respectively. However, if smallest particles <10 nm are excluded from MC-Au-red particle counting because they just have a small contribution (2%, to the area covered by individual particles) diameter results in 173 nm.

Figure 4 depicts Hg breakthrough curves for sorbents and Table 2 reports the total amount of Hg captured by sorbents, calculated from the integration of the breakthrough curves, when reached 95% saturation, deducing death volume of the reactor and the contribution of the supports. Carbonaceous materials can exhibit

some mercury capture by either physisorption or chemisorption mechanism. In present case, carbon supports (after a TTR similar to that undergone by sorbents) exhibited very low Hg adsorption capacity, less than 0.5 μg Hg/g support. This is in agreement with results in the literature concerning with the low affinity between non-treated activated carbons and elemental mercury [20, 21]. This value was subtracted from value obtained from breakthrough curve integration. Because of the on-line mercury analyzer determines only elemental mercury (that is the only specie fed to the gas), in some duplicated experiments the possible oxidation of elemental mercury by Au catalytic oxidation was followed. The train of impingers containing a chilled solution of $KMnO_4/H_2SO_4$ and chilled solution of KCl was placed after the mercury analyzer in order to retain elemental and oxidized mercury, respectively (the so-called Ontario-Hydro ASTM method). Both solutions were further analyzed in the AMA. No oxidized mercury was detected in any of the impinger analyzed.

It can be observed in Figure 4 that breakthrough times are larger for MC-Au-red sorbent than that for MC-Au-col. On the other hand, it seems that temperature influences in more extent on MC-Au-col breakthrough curve. However, magnification of MC-Au-red breakthrough curve shows also some differences with temperature. Moreover, the amount of Hg captured is higher for MC-Au-red as can be deduced from Table 2. This fact can be attributed to the different Au content of both sorbents, as it is shown below. Work on Hg capture at different temperatures was carried out by some authors [22], but the use of thin films of Au instead particles and low temperatures and low Hg initial concentration limits the extrapolation of those results. Figures 5 and 6 show the Hg retention capacity by Au content of each sorbent and the Hg retention efficiency for MC-Au-red and MC-Au-col, respectively, for 20% and 80% breakthrough at different temperatures. As can be observed in Figures 5 and 6,

it seems that the degree of Au use is similar for both sorbents despite of both methodologies of Au deposition give different Au particle size and both sorbents reached up to 20 mg Hg/g Au, depending on the temperature. This fact seems a contradiction because there is an overwhelming evidence of the dependence of Au particle size and its characteristics related to the defects on the crystal structure. However, the average Au particle size for our sorbents is far from that reported in the literature which maximize the effect of particle size on structural defects of the Au crystal [23]. In present case, the independence of particle size on the Hg retention could be explained as follows: the high Au particle size for both sorbents does not make differences on Au crystal structure and consequently, no differences are found in Hg capture performance. Despite of particle size of present sorbents is more than four times the particle size that takes advantage of the increase of Au atoms with different coordination number, the Hg capture efficiency at saturation is higher than that reported in reference [24] for a gold-activated carbon based sorbent and the amount of Hg captured is higher than that reported by reference [25] for Ag based sorbent and by reference [26] for Ag based sorbent containing 20% Ag.

The highest temperature used for Hg retention gives the lowest Hg retention capacity. This fact can be related with the low temperature needed to regenerate the sorbents, which was 220ºC [15]. Once the sorbent is exhausted, a Hg-TPD experiment (Figure 7) was carried out at a heating rate of 10ºC/min. It was found that temperature for maximum Hg evolution was around 220ºC. However, Hg evolution started near 180ºC, which is close enough to the retention temperature of 150ºC. This effect is more pronounced for sorbent MC-Au-col, because the Hg evolution in Hg-TPD experiments takes place at a slightly lower temperature than that for sorbent MC-Au-red.

Both Hg capture capacity and Hg capture efficiency were determined along several cycles of retention-regeneration on sorbent MC-Au-red. Temperature of 75ºC for retention experiments was selected among those studied because highest Hg retention performance was obtained for this sorbent. The conditions for regeneration have been detailed in the experimental section.

Figure 8 shows the Hg retention capacity and efficiency along several retention-regeneration cycles. The Hg retention efficiency is maintained along cycles, indicating that the sorbent does not undergo significant changes after regeneration. On the other hand, the amount of Hg retained at 20% and 80% breakthrough decreases slightly after first regeneration and it is maintained along the cycles. This fact cannot be attributed to incomplete Hg evolution at 220ºC as can be seen in Figure 9. This fact can be explained in terms of Hg-TPD experiments (Figure 7).

A maximum of Hg evolution is found near 220ºC, but a shoulder can be found at higher temperatures, indicating that not only Hg amalgamation is the mechanism for Hg capture but also other Hg retention mechanism is involved, being chemisorption on the carbon material of the support the most probable mechanism. However, the amount of Hg evolved at higher temperatures is low to justify the use of higher regeneration temperatures to completely remove Hg. But this chemisorbed Hg remains on the sorbent after regeneration at 220ºC, meaning that no Hg will be retained by this mechanism after regeneration, because chemisorption sites are still occupied. This fact could explain the slight loss in Hg retention capacity after first regeneration. However, after first cycle the amount of Hg retained is similar to the amount retained in the rest of the cycles tested, because the amalgamation capacity is maintained and the sites for chemisorption are yet occupied.

More Hg capture-regeneration cycles are expected to maintain the behavior observed for firsts five cycles, because mercury capture via amalgamation can be regenerated for unlimited times in theory [27].

To support this theory, sorbents were characterized after Hg capture, before regeneration. The XRD pattern (Figure 10) of sample MC-Au-red before the exposition to Hg exhibits the peaks expected for gold (according to the Joint Committee on Powder Diffraction Standards data bank) occurring at about 38.2º, 44.4º, 64.6º and 77.6º in 2θ. They correspond to gold (1 1 1), (2 2 0), (2 2 0) and (3 1 1) planes, respectively. The peak intensity of the (1 1 1) plane parallel to the carbon surface is high as corresponds to the preferred orientation for polycrystalline fcc (face-centered cubic) metals deposited onto amorphous substrates. The intensity of the rest of the peaks is low due to the low Au content of the sample. This is the reason of peak at around 81.7º, corresponding to (2 2 2) plane is not shown because is almost negligible. The band around 2θ=44º is attributed to carbon signal of plane (0 0 1) diffraction.

After Hg exposition, a new diffractogram was obtained on sample MC-Au-red. As can be seen in Figure 10, the exposition to mercury has not changed the XRD pattern of gold. As it was previously discussed [15] the mercury capture on the Au/C sorbent is based on the amalgam mechanism, so displacement of Au peaks was expected because of the formation of Au-Hg amalgam [28]. However, in present case the relation Hg/Au (=0.02) is low and this should be the reason of no new peaks appearing and no intensity of peaks decreasing. Assuming that the most probable Au-Hg amalgam formed is Au_3Hg (relation Hg/Au 0.33), the Au capacity for Hg of sorbent is not reached by far. This fact could confirm the need of lower Au particle

size to take advantage of points of defects on Au crystal structure where Hg can be adsorbed.

Because of XRD is a bulk technique and it is difficult to follow changes when concentration of sample elements are low, the study of the surface of sample MC-Au-red before Hg exposition, after Hg exposition and after in-situ regeneration at 220ºC was carried out by XPS. Binding energy regimes containing the Au $4f_{5/2}$ y Au $4f_{7/2}$ emission lines and Hg $4f_{5/2}$ y Hg $4f_{7/2}$ emission lines were obtained. Table 3 reports XPS peaks after curve fitting. The position of peaks corresponding to Au^0 and $Au^{\delta+}$ after Hg exposition is slightly shifted to higher binding energies. This shift has been reported by others [29] related with the amalgam formation. Hg content is at% 0.13 and Au content is at% 5.25, resulting in a Hg/Au ratio of 0.025, close to that obtained from breakthrough curves, as it has been reported above.

Once the Hg and Au XPS spectra have been acquired, sample was heated up in situ at 220ºC during 2 h to remove Hg from sorbent. After cooling down to room temperature, a new XPS spectrum was obtained in order to follow possible changes on Au emission line. As can be seen in Table 3, no displacement of peaks position from fresh sample is observed, indicating that Au/C sorbent is not altered by Hg capture-regeneration. These results agree with those obtained from breakthrough curves along Hg capture-regeneration cycles.

CONCLUSIONS

A novel structured regenerable sorbent for Hg capture based on Au/C has been developed. The procedure for sorbent preparation is based on the direct reduction of

an Au salt on a carbon monolith without the addition of reducing or protective chemicals, which represents a novelty respect to the gold colloidal method.

This sorbent with an Au content of 0.11% exhibits a high Hg retention efficiency in a range of temperatures from 50ºC to 150ºC. The efficiency is maintained along several Hg retention-regeneration cycles with regeneration temperatures as low as 220ºC.

There is a differentiated Hg chemisorption and amalgamation mechanism on Au/C sorbents during first capture-regeneration cycle. After first cycle, the chemisorption sites are occupied and the Hg capture through amalgamation mechanism is maintained along several cycles.

The in-situ XPS and XRD studies explain the theoretically unlimited cycles of Hg-Au amalgamation and regeneration: after regeneration Au on sorbent exhibit same XPS behavior than that for fresh sorbent.

ACKNOWLEDGEMENTS

The financial support from Spanish Ministry of Science and Innovation and European Regional Development Funds (ref: ENE2011-23412) is duly recognized. C. Gómez-Giménez wants to thank CSIC and European Regional Development Funds for JAE grant.

REFERENCES

[1] The Global Atmospheric Mercury Assesment: Sources, Emissions and Transport., in, UNEP-Chemicals, Geneva, Switzerland, 2008.
[2] S. Pye, G. Jones, R. Stewart, M. Woodfield, K. Kubica, R. Kubica, J. Pacyna, Costs and environmental effectiveness of options for reducing mercury emissions to air from small-scale

combustion installations, AEAT/ED48706/Final Report, AEA Technology Environment (Ed.) Harwell, Oxon, UK, 2006.
[3] E.S. Olson, B.A. Mibeck, Oxidation Kinetics and the Model for Mercury Capture on Carbon in Flue Gas, in: Internation Conference on Air Quality, Arlington, VA, USA, September 19-21, 2005.
[4] A. Stergarsek, M. Horvat, J. Kotnik, J. Tratnik, P. Frkal, D. Kocman, R. Jacimovic, V. Fajon, M. Ponikvar, I. Hrastel, J. Lenart, B. Debeljak, M. Cujez, The role of flue gas desulphurisation in mercury speciation and distribution in a lignite burning power plant, Fuel, 87 (2008) 3504-3512.
[5] J. Kilgroe, C.B. Sedman, R. Srivastava, C.L. Ryan, S. Thorneloe, Control of mercury emissions from coal-fired electric utility boilers: interim report, EPA 600/R-01-109 U.S. Environmental Protection Agency., Washington, D.C., USA, 2001.
[6] H. Stuhler, S.C. Amendola, Efficient removal of mercury from flue gases, US Patent 20060120935 (2006).
[7] S. Long, D. Scott, R. Thompson, Atomic-Absorption Determination of Elemental Mercury Collected from Ambient Air on Silver Wool, Anal. Chem., 45 (1973) 2227-2233.
[8] R. Nowakowski, T. Kobiela, Z. Wolfram, R. Dus, Atomic force microscopy of Au/Hg alloy formation on thin Au films, Appl. Surf. Sci., 115 (1997) 217-231.
[9] F.H. Schaedlich, D.R. Schneeberger, Cartridge for Collection of a Sample by Adsorption onto a Solid Surface, US Patent 5660795 (1997).
[10] C. Battistoni, E. Bemporad, A. Galdikas, S. Kaciulis, G. Mattogno, S. Mickevicius, V. Olevano, Interaction of mercury vapour with thin films of gold, Appl. Surf. Sci., 103 (1996) 107-111.
[11] J. Turkevich, P.C. Stevenson, J. Hillier, A Study of the Nucleation and Growth Processes in the Synthesis of Colloidal Gold, Discuss. Faraday Soc., (1951) 55-75.
[12] S. Dong, P.-J. Li, C. Tang, Preparation, characterization and application of carbon-supported gold catalyst, Conference Proceedings - 30th International Precious Metals Institute, Las Vegas, USA, 2006, pp. 1-7.
[13] R. Juan, M.T. Izquierdo, B. Rubio, C. Ruiz, D. Ballestero, Sorbente regenerable de Au/monolito de carbono para la retención de mercurio elemental en fase gas., ES Patent 201132136 (2011).
[14] T. Muangnapoh, N. Sano, S.-I. Yusa, N. Viriya-empikul, T. Charinpanitkul, Facile strategy for stability control of gold nanoparticles synthesized by aqueous reduction method, Curr. Appl. Phys., 10 (2010) 708-714.
[15] M.T. Izquierdo, D. Ballestero, R. Juan, E. Garcia-Diez, B. Rubio, C. Ruiz, M. Pino, Tail-end Hg capture on Au/carbon-monolith regenerable sorbents, J. Hazar. Mat., 193 (2011) 304-310.
[16] A.M. Visco, F. Neri, G. Neri, A. Donato, C. Milone, S. Galvagno, X-ray photoelectron spectroscopy of Au/Fe_2O_3 catalysts, Phys. Chem. Chem. Phys., 1 (1999) 2869-2873.
[17] S. Minico, S. Scire, C. Crisafulli, S. Galvagno, Influence of catalyst pretreatments on volatile organic compounds oxidation over gold/iron oxide, Appl. Catal. B-Environ., 34 (2001) 277-285.
[18] C.N.R. Rao, V. Vijayakrishnan, H.N. Aiyer, G.U. Kulkarni, G.N. Subbanna, An investigation of well-characterized small gold clusters by photoelectron-spectroscopy, tunneling spectroscopy, and cognate techniques, J. of Phys. Chem., 97 (1993) 11157-11160.
[19] D.A. Bulushev, I. Yuranov, E.I. Suvorova, P.A. Buffat, L. Kiwi-Minsker, Highly dispersed gold on activated carbon fibers for low-temperature CO oxidation, J. Catal., 224 (2004) 8-17.

[20] F.E. Huggins, N. Yap, G.P. Huffman, C.L. Senior, XAFS characterization of mercury captured from combustion gases on sorbents at low temperatures, Fuel Proc. Technol., 82 (2003) 167-196.
[21] B. Padak, J. Wilcox, Understanding mercury binding on activated carbon, Carbon, 47 (2009) 2855-2864.
[22] M. Levlin, E. Ikavalko, T. Laitinen, Adsorption of mercury on gold and silver surfaces, Fresenius J. Anal. Chem., 365 (1999) 577-586.
[23] S. Schimpf, M. Lucas, C. Mohr, U. Rodemerck, A. Bruckner, J. Radnik, H. Hofmeister, P. Claus, Supported gold nanoparticles: in-depth catalyst characterization and application in hydrogenation and oxidation reactions, Catal. Today, 72 (2002) 63-78.
[24] J. Rodriguez-Perez, M. Antonia Lopez-Anton, M. Diaz-Somoano, R. Garcia, M. Rosa Martinez-Tarazona, Development of Gold Nanoparticle-Doped Activated Carbon Sorbent for Elemental Mercury, Energy & Fuels, 25 (2011) 2022-2027.
[25] T.Y. Yan, A novel process for Hg removal from gases, Ind. & Eng. Chem. Res., 33 (1994) 3010-3014.
[26] Y. Liu, D.J.A. Kelly, H. Yang, C.C.H. Lin, S.M. Kuznicki, Z. Xu, Novel regenerable sorbent for mercury capture from flue gases of coal-fired power plant, Environ. Sci. & Technol., 42 (2008) 6205-6210.
[27] E.J.P. Granite, H.W., R.A. Hargis, Sorbents for mercury removal from flue gas, in, DOE/FETC/TR-98-01, Pittsburg, USA, 1998.
[28] T. Kobiela, B. Nowakowski, R. Dus, The influence of gas phase composition on the process of Au-Hg amalgam formation, App. Surf. Sci., 206 (2003) 78-89.
[29] J. Thome, M. Himmelhaus, M. Zharnikov, M. Grunze, Increased lateral density in alkanethiolate films on gold by mercury adsorption, Langmuir, 14 (1998) 7435-7449.

FIGURE CAPTIONS

Figure 1. Au 4f XPS and fitted spectra of samples MC-Au-red and MC-Au-col before and after TTR.

Figure 2. FE-SEM micrographs of sample MC-Au-red before (left) and after (right) TTR.

Figure 3. FE-SEM micrographs (after TTR) of samples MC-Au-red (left) and MC-Au-col (right) and particle size distribution from Image J analysis.

Figure 4. Hg breakthrough curves for sorbents obtained at different temperatures and $W_{Au}/Q=2.9x10^{-5}$ g h l^{-1}.

Figure 5. Hg retention capacity and Hg retention efficiency for MC-Au-red at different temperatures and $W_{Au}/Q=2.9x10^{-5}$ g h l^{-1}.

Figure 6. Hg retention capacity and Hg retention efficiency for MC-Au-col at different temperatures and $W_{Au}/Q=2.9x10^{-5}$ g h l^{-1}.

Figure 7. Hg evolution from exhausted sorbents in Hg-TPD experiments

Figure 8. Hg retention capacity and efficiency for MC-Au-red along several capture-regeneration cycles (temperature for capture step 50ºC; temperature for regeneration step 220ºC).

Figure 9. Hg evolution during sorbent regeneration at 220ºC.

Figure 10. XRD of fresh MC-Au-red sorbent and after an experiment of Hg capture.

Table 1. Results from XPS analysis.

Sample	Binding energy (eV) and peak area (%)				*Au_{XPS}
	Au^0		$Au^{\delta+}$		(at. %)
MC-Au-red (before TTR)	84.0 (41.7)	87.7 (37.5)	84.7 (15.6)	88.7 (5.2)	1.18
MC-Au-red (after TTR)	84.0 (51.1)	87.7 (36.6)	84.8 (9.6)	88.8 (2.6)	4.73
MC-Au-col (before TTR)	84.0 (49.6)	87.7 (35.8)	85.2 (10.2)	88.8 (4.4)	1.07
MC-Au-col (after TTR)	84.0 (48.1)	87.7 (40.6)	84.9 (8.1)	89.0 (3.2)	2.96

*considering the only presence of C and Au.

Table 2. Total amount of Hg captured by sorbents (95% breakthrough) from integration of breakthrough curves. In parenthesis values obtained from AMA analysis of a sorbent.

Temperature (ºC)	MC-Au-red	MC-Au-col
	μg Hg/g sorbent	
50	20.5 (19.9)	9.7
75	23.0	7.8
100	21.9	7.8
120	21.0 (21.2)	6.6
150	15.5	3.2

Table 3. Results from XPS analysis on MC-Au-red sorbent after Hg capture experiment ans after in situ regeneration.

Sample	Binding energy (eV)				Au_{XPS}	Hg_{XPS}
	Au^0		$Au^{\delta+}$		(at. %)	(at. %)
MC-Au-red	84.0	87.7	84.8	88.8	4.73	-
MC-Au-red (after Hg exp)	84.1	87.8	84.9	88.9	5.25	0.13
MC-Au-red (after regeneration)	84.0	87.7	84.8	88.8	5.60	-

Figure 1

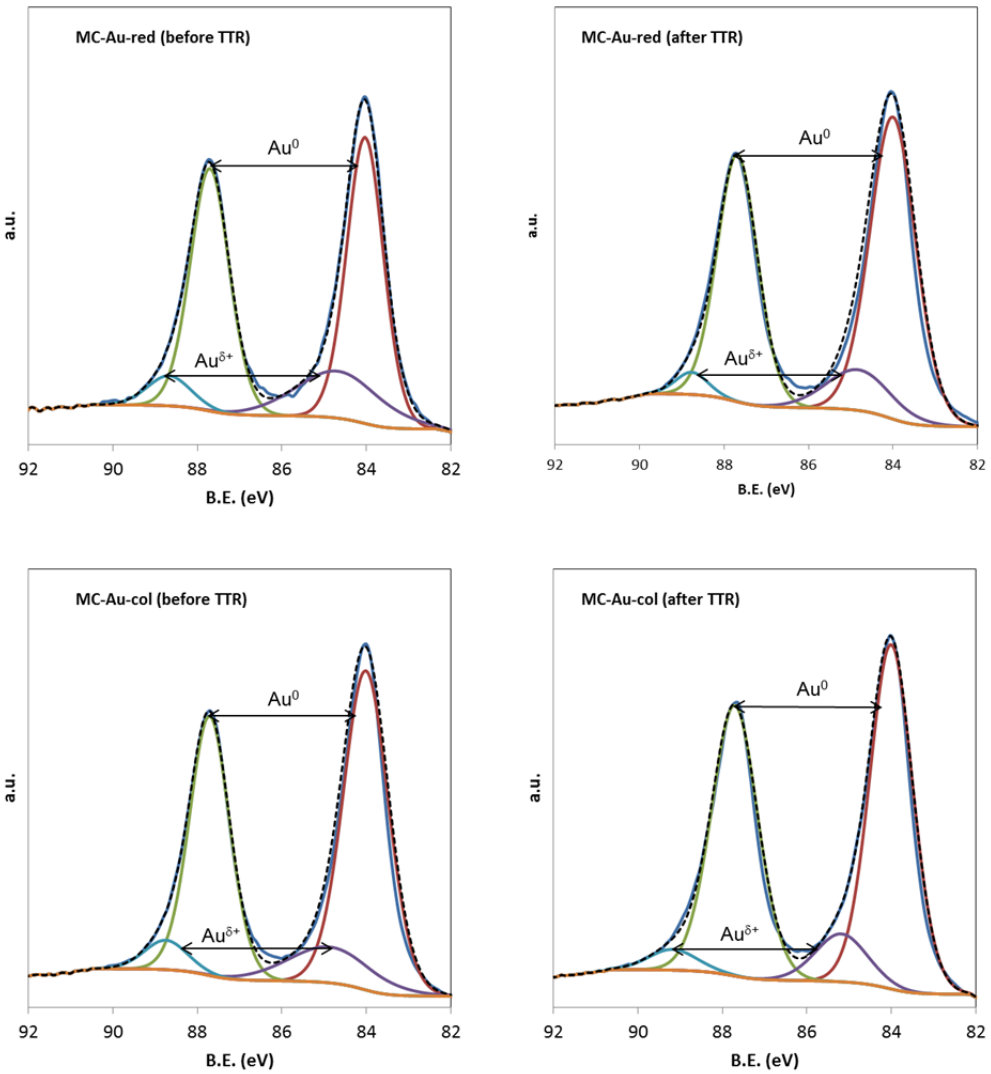
MC-Au-red (before TTR)
MC-Au-red (after TTR)
MC-Au-col (before TTR)
MC-Au-col (after TTR)
Au0
Auδ+
a.u.
92
90
88
86
84
82
B.E. (eV)

Figure 2

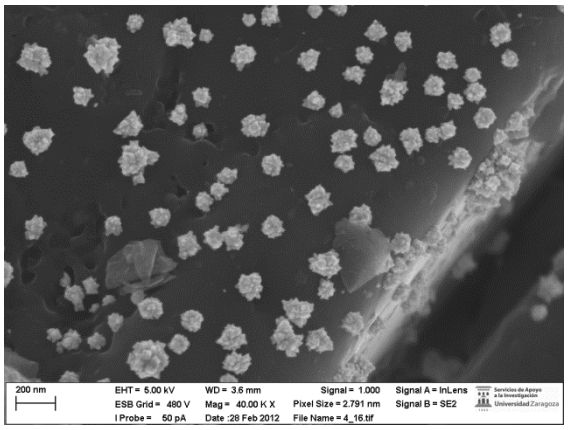
200 nm
EHT = 5.00 kV
WD = 3.6 mm
Signal = 1.000
Signal A = InLens
ESB Grid = 480 V
Mag = 40.00 K X
Pixel Size = 2.791 nm
Signal B = SE2
I Probe = 50 pA
Date :28 Feb 2012
File Name = 4_16.tif
Universidad Zaragoza

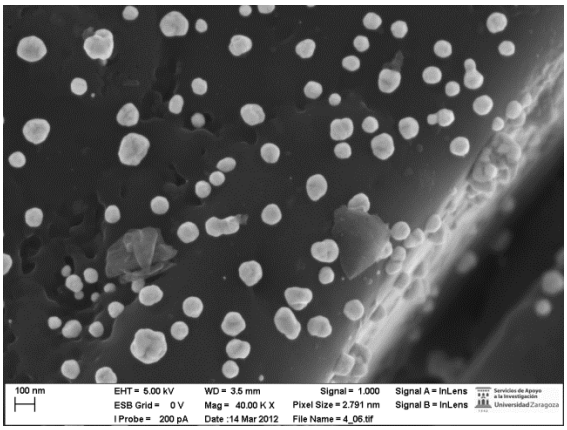
100 nm
EHT = 5.00 kV
WD = 3.5 mm
Signal = 1.000
Signal A = InLens
ESB Grid = 0 V
Mag = 40.00 K X
Pixel Size = 2.791 nm
Signal B = InLens
I Probe = 200 pA
Date :14 Mar 2012
File Name = 4_06.tif
Universidad Zaragoza

Figure 3

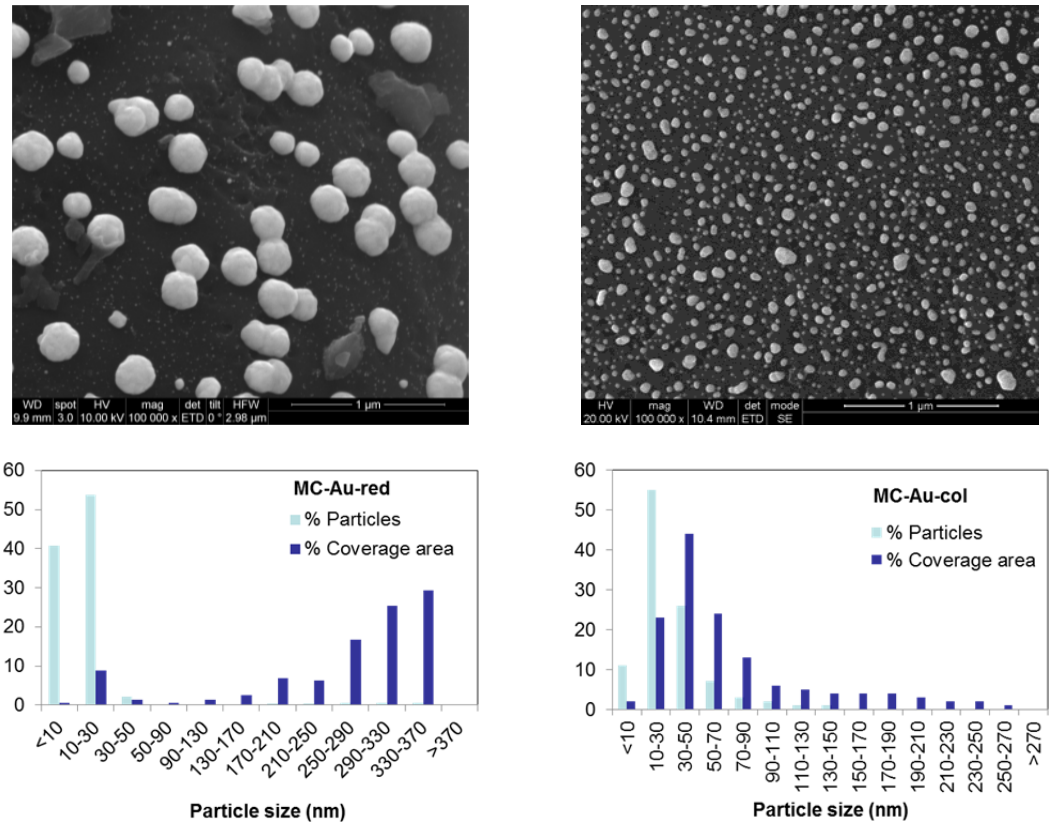
WD spot HV mag det tilt HFW
9.9 mm 3.0 10.00 kV 100 000 x ETD 0 ° 2.98 µm
1 µm
HV mag WD det mode
20.00 kV 100 000 x 10.4 mm ETD SE
1 µm
MC-Au-red
% Particles
% Coverage area
60
50
40
30
20
10
0
<10
10-30
30-50
50-90
90-130
130-170
170-210
210-250
250-290
290-330
330-370
>370
Particle size (nm)
MC-Au-col
% Particles
% Coverage area
60
50
40
30
20
10
0
<10
10-30
30-50
50-70
70-90
90-110
110-130
130-150
150-170
170-190
190-210
210-230
230-250
250-270
>270
Particle size (nm)

Figure 4

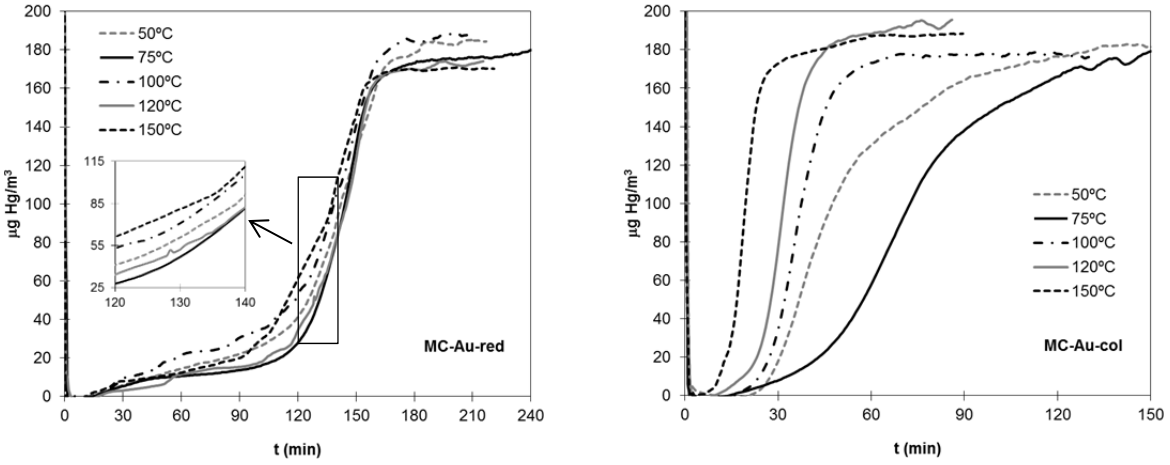

Figure 5

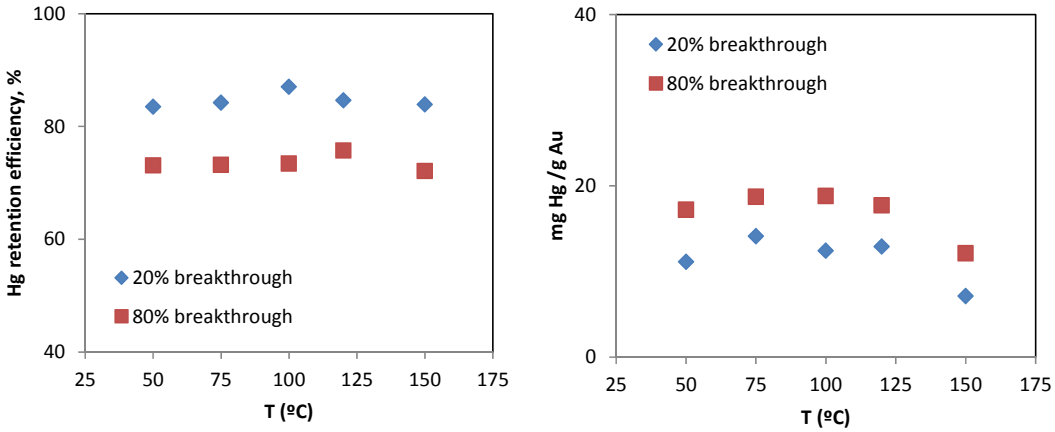
Hg retention efficiency, %
100
80
60
40
20% breakthrough
80% breakthrough
25
50
75
100
125
150
175
T (ºC)
mg Hg / g Au
40
20
0
20% breakthrough
80% breakthrough
25
50
75
100
125
150
175
T (ºC)

Figure 6

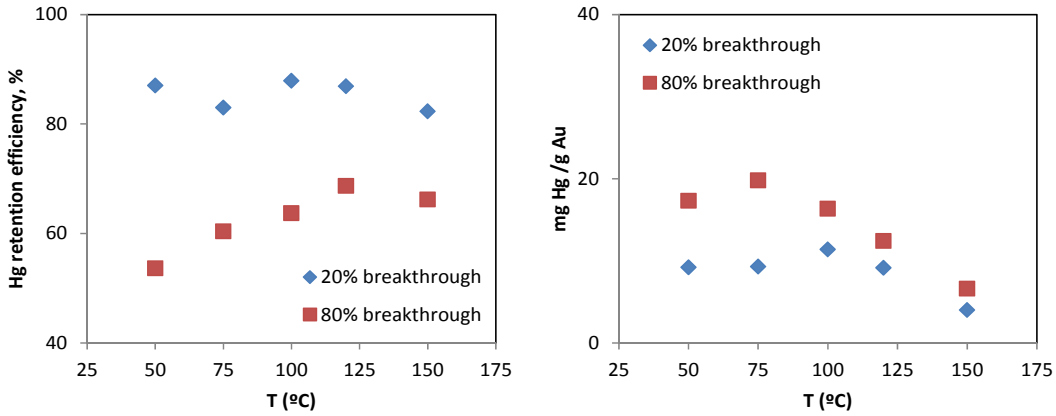
Hg retention efficiency, %
100
80
60
40
25
50
75
100
125
150
175
T (ºC)
20% breakthrough
80% breakthrough
mg Hg / g Au
40
20
0
25
50
75
100
125
150
175
T (ºC)
20% breakthrough
80% breakthrough

Figure 7

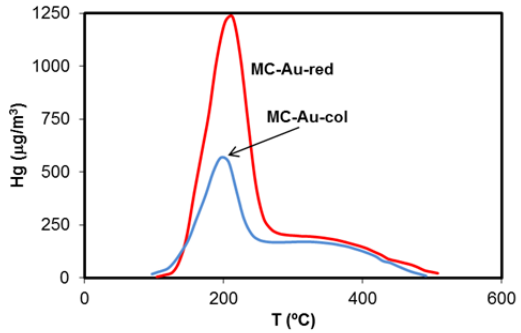
1250
1000
750
500
250
0
Hg (µg/m³)
MC-Au-red
MC-Au-col
0
200
400
600
T (ºC)

Figure 8

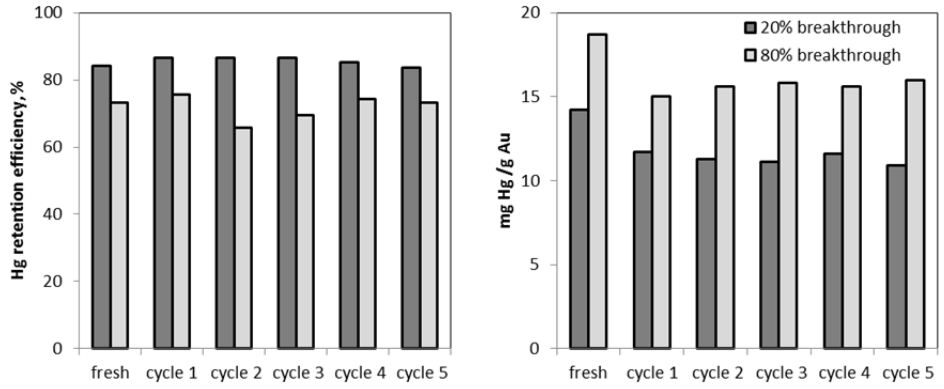
Hg retention efficiency, %
100
80
60
40
20
0
fresh
cycle 1
cycle 2
cycle 3
cycle 4
cycle 5
mg Hg /g Au
20
15
10
5
0
20% breakthrough
80% breakthrough
fresh
cycle 1
cycle 2
cycle 3
cycle 4
cycle 5

Figure 9

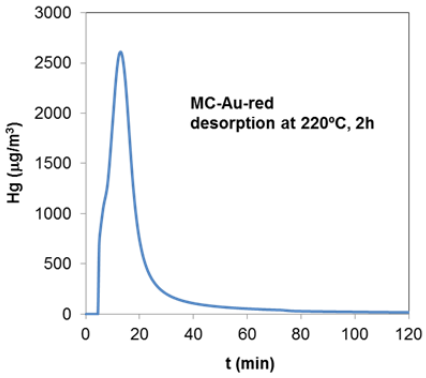
MC-Au-red
desorption at 220°C, 2h
Hg (µg/m³)
t (min)
3000
2500
2000
1500
1000
500
0
0
20
40
60
80
100
120

Figure 10

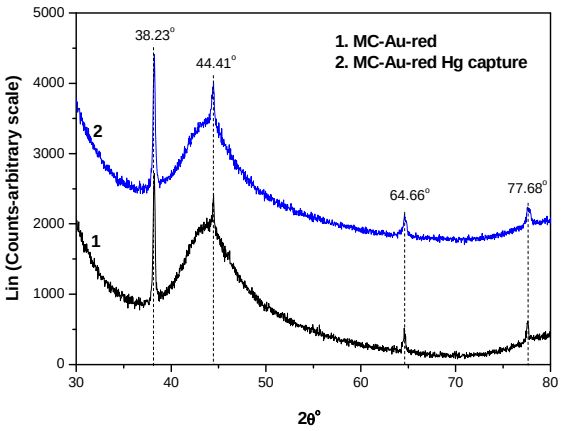
1. MC-Au-red
2. MC-Au-red Hg capture
38.23°
44.41°
64.66°
77.68°
2
1
Lin (Counts-arbitrary scale)
2θ°
5000
4000
3000
2000
1000
0
30
40
50
60
70
80